Science of the Total Environment 645 (2018) 1065–1082

Contents lists available at ScienceDirect

Science of the Total Environment

journal homepage: www.elsevier.com/locate/scitotenv

Analysis of future climate change impacts on snow distribution over mountainous watersheds in Northern California by means of a physically-based snow distribution model

K. Ishida [a,*], A. Ercan [b], T. Trinh [a], M.L. Kavvas [c], N. Ohara [d], K. Carr [b], M.L. Anderson [e]

[a] Hydrologic Research Laboratory, Department of Civil and Environmental Engineering, University of California, Davis. One Shields Avenue, Davis, CA 95616, USA
[b] J. Amorocho Hydraulics Laboratory, Department of Civil and Environmental Engineering, University of California, Davis. One Shields Avenue, Davis, CA 95616, USA
[c] Hydrologic Research Laboratory and J. Amorocho Hydraulics Laboratory, Department of Civil and Environmental Engineering, University of California, Davis. One Shields Avenue, Davis, CA 95616, USA
[d] Civil and Architectural Engineering, University of Wyoming, Laramie, WY 82071, USA
[e] State Climatologist, California Department of Water Resources, Sacramento, CA 95821, USA

HIGHLIGHTS

- Snow conditions over three watersheds in California for 2010–2100 were projected.
- A physically-based snow model was used to simulate future snow conditions.
- The downward trend in snowpack is significant over nearly the entire watersheds.
- Snowpack reduction is large at high elevation areas during the snow melting period.

GRAPHICAL ABSTRACT

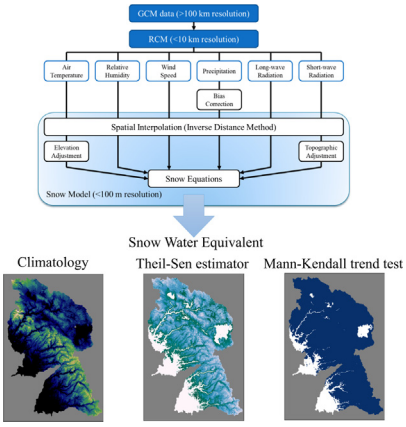

ARTICLE INFO

Article history:
Received 11 May 2018
Received in revised form 13 July 2018
Accepted 18 July 2018
Available online 20 July 2018

Editor: D. Barcelo

Keywords:
Snow distribution
Future climate projections
Physically-based snow model
Dynamical downscaling

ABSTRACT

The impacts of climate change on snow distribution through the 21st century were investigated over three mountainous watersheds in Northern California by means of a physically-based snow distribution model. The future climate conditions during a 90-year future period from water year 2010 to 2100 were obtained from 13 future climate projection realizations from two GCMs (ECHAM5 and CCSM3) based on four SRES scenarios (A1B, A1FI, A2, and B1). The 13 future climate projection realizations were dynamically downscaled at 9 km resolution by a regional climate model. Using the downscaled variables based on the 13 future climate projection realizations, snow distribution over the Feather, Yuba, and American River watersheds (FRW, YRW, and ARW) was projected by means of the physically-based snow model. FRW and YRW watersheds cover the main source areas of the California State Water Project (SWP), and ARW is one of the key watersheds in the California Central Valley Project (CVP). SWP and CVP are of great importance as they provide and regulate much of the California's water for drinking, irrigation, flood control, environmental, and hydro-power generation purposes. Ensemble average snow distribution over the study watersheds was calculated over the 13 realizations and for each scenario,

* Corresponding author at: Department of Civil and Environmental Engineering, Kumamoto University, 2-39-1 Kurokami, Kumamoto 860-8555, Japan.
E-mail addresses: keiishida@kumamoto-u.ac.jp (K. Ishida), aercan@ucdavis.edu (A. Ercan), tqtrinh@ucdavis.edu (T. Trinh), mlkavvas@ucdavis.edu (M.L. Kavvas), nohara1@uwyo.edu (N. Ohara), kjcarr@ucdavis.edu (K. Carr), manderson@water.ca.gov (M.L. Anderson).

https://doi.org/10.1016/j.scitotenv.2018.07.250
0048-9697/© 2018 Elsevier B.V. All rights reserved.

revealing differences among the scenarios. While the snow reduction through the 21st century was similar between A1B and A2, the snow reduction was milder for B1, and more severe for A1FI. A significant downward trend was detected in the snowpack over nearly the entire watershed areas for all the ensemble average results.
© 2018 Elsevier B.V. All rights reserved.

1. Introduction

Snow regime is a large concern for watershed management in many regions in the world because snow melt can be an important water resource during the warm season. Precipitation is the major water input to a watershed. If the watershed is located in a cold region, or covers sufficiently high mountainous areas, some portion of precipitation falls as snow during cold season. Snowfall accumulates as snowpack throughout the cold season, and gradually melts during the warm season. As such, snowpack can store large volumes of water, releasing water during the warm season. Global climate change is widely recognized as summarized in a report by Intergovernmental Panel on Climate Change (2013). Since snow accumulation and melt processes are very sensitive to air temperature (Martinec, 1960; Martinec and Rango, 1981; Rango and Martinec, 1995; Cline, 1997; Burnett et al., 2003), snow regime may change under a changing climate in the future. Therefore, it is crucial for watershed management to investigate the impacts of climate change on snow regime in the future.

Future climate projections, which are obtained from the simulations of global climate models (GCMs) under various future climate scenarios, are frequently utilized for the analysis of future climate change impacts. GCMs simulate the atmospheric-land-oceanic processes, including the precipitation process, for the whole globe. Because such a simulation requires large computational power, a typical horizontal grid resolution is between 1 and 2 degrees (Flato et al., 2013). Due to their coarse resolution, GCMs cannot reliably reflect precipitation over land regions with steep terrain. Therefore, downscaling of the climate projections of GCMs to a finer resolution for regional water balance studies is generally required to obtain reliable precipitation.

There are two major downscaling techniques: statistical downscaling and dynamical downscaling. Statistical downscaling uses statistics obtained from empirical relationships between GCM modeled large-scale atmospheric variables and observed local-scale meteorological variables. Because of its lighter technical and computational demands, statistical downscaling is quick and inexpensive. However, statistical downscaling can generally be applied to only precipitation and air temperature due to the limited availability of observation data. There are several studies on the snow regime in the future based on future climate projections. Some of them are focused on snowfall frequency or snow/rain ratio (Pons et al., 2009; McAfee et al., 2014), which require only precipitation and air temperature for their calculation. Others employ only a regression model (Castebrunet et al., 2014; Khadka et al., 2014) or a simple hydrologic/snow model (Dettinger et al., 2004; Hayhoe et al., 2004; Maurer, 2007) that requires only precipitation and air temperature.

Dynamical downscaling is a technique to downscale atmospheric variables by means of a regional climate model (RCM). Due to the use of a RCM, dynamical downscaling can provide a detailed and comprehensive representation of orographic effects, land-sea contrast, and land surface characteristics (Jones et al., 1995; Christensen and Christensen, 2007). Meanwhile, the dynamical downscaling technique is capable of producing outputs at finer temporal resolutions, such as at hourly time-scale. Furthermore, dynamical downscaling can produce not only precipitation and air temperature but also other variables such as humidity, wind field, and radiation, which are required for detailed snow accumulation and melting process modeling. However, dynamical downscaling has a significant disadvantage due to its required computational demands. As such, dynamical downscaling has been rarely used to obtain inputs to snow regime modeling. Bavay et al. (2009) utilized dynamically downscaled variables obtained from the PRUDENCE (Prediction of Regional scenarios and Uncertainties for Defining European Climate Change Risks and Effects) project (Christensen et al., 2007) to simulate the snow regime during the late 21st century (2071–2100) by means of a distributed snow model, Alpine3D. These researchers utilized daily minimum and maximum air temperature, daily precipitation, and daily average longwave radiation which is the only additional variable (longwave radiation) when compared to studies using statistical downscaling. Other variables, such as humidity, wind field, and shortwave radiation, were not taken into consideration although they may influence the snow regime. More recently, Trinh et al. (2017) investigated future climate change impacts on the total snow budget over the Shasta Dam watershed in California. They utilized a physically-based snow model with dynamically downscaled variables so that not only precipitation and air temperature but also humidity, wind field, and shortwave radiation can be taken into consideration.

The main objective of this study is to investigate the impacts of climate change on snow distribution over three study watersheds in Northern California by means of a physically-based snow model that takes into account not only precipitation and air temperature but also humidity, wind field, and longwave and shortwave radiation. The variables required by the physically-based snow model were obtained from dynamically downscaled future climate projection realizations. As in Trinh et al. (2017), this study considered 13 future climate projection realizations from two GCMs (ECHAM5 and CCSM3) based on four future emission scenarios although most of the aforementioned future snow studies utilized only a few realizations. The 13 future climate projection realizations were dynamically downscaled by a RCM during the 90 water years (wy2010–2100). The physically-based snow model was run with the dynamically-downscaled future climate projection realizations as inputs. Then, the ensemble average of snow water equivalent was calculated over all the realizations and over each emission scenario.

The study presented herein investigates the future climate change impacts on snow distribution, in detail, over three watersheds, the American River watershed (ARW), the Yuba River watershed, and the Feather River watershed in Northern California, while Trinh et al. (2017) focused on the total snow budget over the Shasta Dam watershed in Northern California. ARW is one of the key watersheds of the Central Valley Project, and the YRW and FRW are the main source areas of the California State Water Project. In order for the model to provide reliable and detailed results on snow distribution, it must be capable of reasonably simulating the snow regime throughout the study watersheds. To assess such model capability, this study employs a challenging calibration and validation process on the selected snow model. Initially, one gauging observation station is selected from each of the three watersheds. The snow model is then calibrated by comparing the simulated snow water equivalent with the corresponding observations at the select three observation stations. Following calibration of model parameters at the three observation stations, the snow model is then validated at all the available gauging stations within the three study watersheds.

Once the model is validated, the distribution of the 30-year averaged snow water equivalent in January, March, and May is displayed at 100 m spatial resolution during the early (wy2010–2040), the middle (wy2040–2070), and the late 21st century (wy2070–2100). Snow covered areas and snow water equivalent during these three periods are examined for five divided elevation ranges over the three study

watersheds in order to analyze differences in the future climate change impacts on snow regime among different elevations. Furthermore, trends on the ensemble averages of snow water equivalent for the three selected watersheds were analyzed at each simulation grid by means of the Theil–Sen estimator and the Mann-Kendall trend test to detect spatial differences of future climate change impacts on snow regime. In general, future climate change impacts on snow distribution are investigated by comparing snow water equivalent or snow depth among different future periods. However, because trend analysis requires statistical proof of trends in a variable under a changing climate, grid-based trend analysis with the Theil-Sen estimator and the Mann-Kendall trend test have been applied in this and other climate change studies (e.g. Kumar et al., 2013; Fischer and Knutti, 2014; Bilbao et al., 2015; Carson et al., 2016). In addition to the analysis of the ensemble average of the snow water equivalent over all 13 future climate projections, the ensemble average of snow water equivalent over each scenario is examined to investigate differences in future climate change impacts on snow distribution among future climate scenarios. The findings of this study may shed light on snow distribution and availability over these three key watersheds in California through the 21st century.

2. Study region

California is located on the west coast of the Unites States, and has two major rivers: the Sacramento River and the San-Joaquin River. The Sacramento River flows from north to south, and the San-Joaquin River flows from south to north. These major rivers converge at the center of an expansive valley region, known as the Central Valley. The Central Valley is bounded on the east by the Sierra-Nevada mountain range. Due to its high elevation peaks, the Sierra-Nevada mountain range has significant snowpack during winter.

The three study watersheds, ARW, YRW, and FRW, are located on the west slope of the Sierra-Nevada mountain range (Fig. 1). The areas of the ARW, the YRW, and the FRW are approximately 4825, 3483, and 9334 km^2, respectively. In elevation, the ARW ranges from 137 m to 3035 m, the YRW from 17 m to 2618 m, and the FRW from 275 m to 2703 m. Annual average precipitation ranges from 584 mm at the valley floor to 1473 mm at the headwaters over the ARW (U.S. Fish and Wildlife Service (USFWS), 1995), from 2032 mm in the upstream area to 508 mm in the downstream area over the YRW (Heiman and Knecht, 2011), and from >2300 mm at the central orographic crest to <500 mm in the eastern headwaters (National Marine Fisheries Service (NMFS), 2000) over the FRW.

In California, a large portion of water resources originate from precipitation over the state's northern region. According to an estimate by the California Department of Water Resources (2003), on average approximately 70% of the state's annual runoff originates north of Sacramento, while about 75% of the State's urban and agricultural water demands are consumed in the southern sector of the state. Meanwhile, approximately 40% of the mean annual runoff north of Sacramento comes from the three study watersheds (Ishida et al., 2015b), rendering them important for water management in California.

Northern California has dry and wet seasons. Most precipitation falls during the wet season from October through April. Usually, the monthly precipitation increases from the beginning of a water year (October) to January. After a peak in January, the monthly precipitation starts to decrease, and there is little precipitation during the dry season between May and September. Higher elevation areas generally have more snowfall in Northern California (Soong and Kim, 1996; Dettinger et al., 2011; Minder et al., 2011; Minder and Kingsmill, 2013). According to Serreze et al. (1999), 67% of precipitation falls as snow over the Sierra Nevada Mountain range. During the cold wet season snow accumulates, and the snowpack reaches its peak value in March or April. Snow melts during the warm dry season. Snow melt is a major water resource during the dry season in California. In fact, some studies estimated that snow melt contributes to 50–80% of runoff during spring and summer in the Central Valley (Stewart et al., 2004; Vicuna and Dracup, 2007; Kapnick and Hall, 2010). Therefore, snow regime over the three study watersheds is a large concern in California.

3. Methodology and models

The snow regime during a 90-year future period from water year 2010 to 2100 was projected at fine spatial resolution by means of the coupled use of a regional climate model (RCM) and a physically-based snow model based on GCM future climate projection realizations. As illustrated in Fig. 2, GCM future climate projection realizations were dynamically downscaled to a 9 km grid resolution over Northern California by means of the RCM. Downscaled atmospheric variables such as air temperature, relative humidity, wind speed, precipitation, and long-wave and short-wave radiation, were utilized as the inputs to a physically-based snow model. The physically-based snow model was then run to simulate the snow regime at a 100 m grid resolution

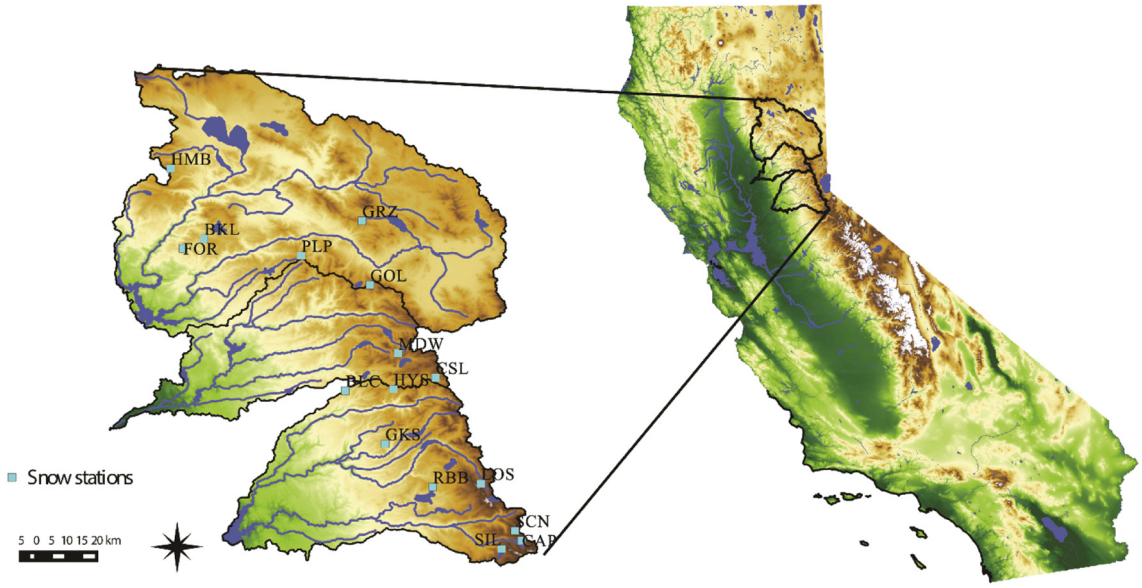

Fig. 1. Plan view of the three study watersheds.

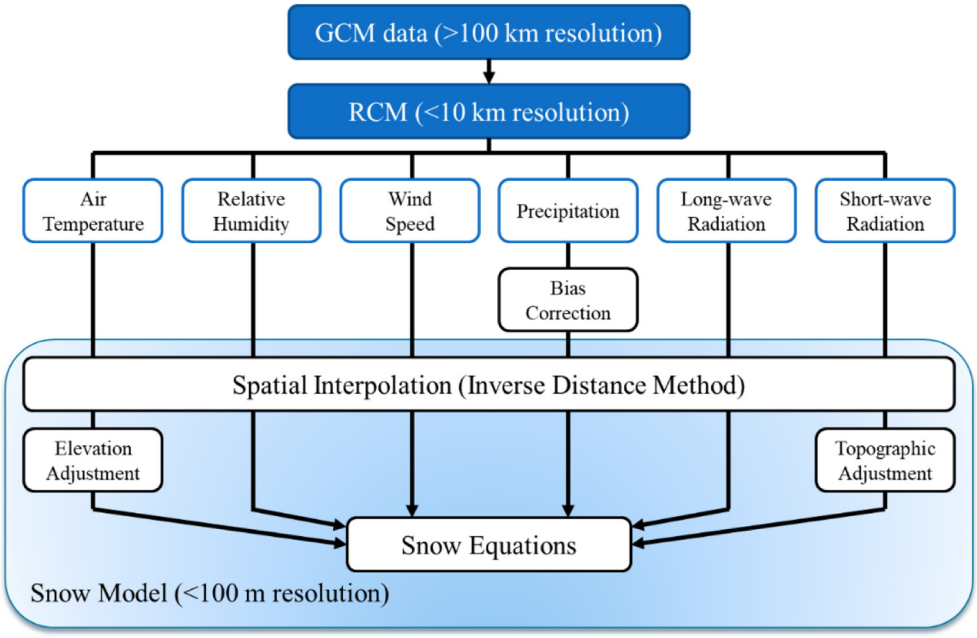

Fig. 2. Data flow for the snow regime projection.

over the three study watersheds in Northern California during the 21st century.

This study employed 13 different future climate projection realizations, which were simulated by two GCMs based on four greenhouse gas emission scenarios of the Special Report on Emissions Scenarios (SRES, Nakicenovic and Swart, 2000). Nine of the 13 realizations are from the fifth-generation global climate model (ECHAM5, Roeckner et al., 2003) by the German Max-Planck Institute (MPI), and the other four are from the third-generation community climate model (CCSM3, Collins et al., 2006) by the University Corporation for Atmospheric Research (UCAR) in the United States. The four SRES scenarios were A1B, A1FI, A2, and B1, which were created based on different assumptions on greenhouse gas emissions, population growth, land use, fossil fuel consumption, as well as economic and technological developments. Among the four scenarios, A1FI is considered to be the worst case scenario, A2 is slightly milder but similar to A1FI, A1B is the most likely scenario, while B1 is the best-case scenario. A complete description of these scenarios can be found in Nakicenovic and Swart (2000). The nine ECHAM5 realizations consist of simulations based on the combination of three SRES scenarios (A1B, A2, and B1) and three different initial conditions, which are referred to as A1B1, A1B2, A1B3, A2-1, A2-2, A2-3, B1-1, B1-2, and B1-3. The realization names represent a SRES scenario with the number of initial conditions. The four CCSM3 realizations come from simulations based on four SRES scenarios (A1B, A1FI, A2, and B1). The four CCSM3 realizations start with only one single initial condition.

The fifth generation Penn State/National Center for Atmospheric Research (NCAR) Mesoscale Model (MM5, Grell et al., 1994) was utilized in order to dynamically downscale the thirteen future climate projection realizations. MM5 has been employed by many research studies on precipitation in the West Coast of the United States (e.g. Colle and Mass, 2000; Mass et al., 2002; Garvert et al., 2005; Moss et al., 2010; Ohara et al., 2011; Lin et al., 2013; Ishida et al., 2015b, 2015c), where the three study watersheds are located. For the dynamical downscaling by MM5, three two-way nested domains were set up: the outer domain with 24×22 horizontal grid points at an 81 km resolution, the second domain with 37×31 horizontal grid points at a 27 km resolution, and the innermost domain with 73×49 horizontal grid points at a 9 km resolution, each with 24 vertical sigma levels. Table 1 describes the model configuration of the MM5 used in this study.

The model biases due to the GCMs' precipitation simulations were corrected before the downscaled atmospheric variables were inputted to the physically-based snow model. In addition to the future climate projection realizations, GCM control runs of the two GCMs (ECHAM5 and CCSM3) were also dynamically downscaled at a 9 km grid resolution over Northern California by means of the MM5 with the aforementioned configuration. Mean monthly basin-average precipitation over each watershed was then calculated for 50 water years (October 1949 through September 1999) from the dynamically downscaled results. To obtain bias correction factors, the mean monthly basin-average precipitation was compared with the corresponding observation data, which was obtained from the Parameter-elevation Relationships on Independent Slopes Model (PRISM; http://prism.oregonstate.edu, Daly et al., 1994; Daly et al., 2008). Finally, the bias correction factors were applied to the dynamically downscaled precipitation for the future period.

As a physically-based snow model, the snow module of the Watershed Environmental Hydrology Model (WEHY) was employed to simulate the snow regime for the 90-year future period in detail. The snow module of the WEHY (WEHY snow model) was developed by Horne and Kavvas (1997), and extended by Ohara and Kavvas (2006) based on the depth-averaged energy balance equations so as to explicitly account for the effect of topography-modified solar radiation on the spatial distribution of snow accumulation and melting processes in addition to evaporation and condensation. Due to its detailed simulation process, this physically-based snow model requires not only precipitation and air temperature, but also relative humidity, wind speed,

Table 1
MM5 model configuration.

Parameterization option	Scheme	Reference
Cloud microphysics processes	Mixed-phase scheme	Reisner et al. (1998)
Cumulus parameterization	Kain-Fritsch scheme	Kain and Fritsch (1993)
Radiation physics	Cloud-radiation scheme	NCAR (2005)
Planetary boundary layer physics	Medium-range forecast scheme	Hong and Pan (1996)
Land surface physics	Five-layer soil model	Dudhia (1996)

and short-wave and long-wave radiation as inputs. Those required variables can be obtained at a finer spatial grid resolution by dynamical downscaling with a RCM. Therefore, the WEHY snow model works well with dynamical downscaling. However, the resolution of the downscaled variables is generally still coarse for detailed snow model simulation. Snow regime is very sensitive to air temperature, and is consequently more sensitive to elevation than precipitation. Topographic aspect affects snow melt caused by radiation. However, the resolution of the RCM grids may not be sufficient to reflect the topographic aspect. In the WEHY snow model, therefore, the atmospheric variables at the RCM grids are interpolated into finer resolution grids by the inverse distance method, and are then adjusted based on the topographic information. Short-wave radiation is adjusted by taking the topographic aspect into consideration, and air temperature is adjusted based on elevation. More detailed information on the WEHY snow model can be found in Ohara and Kavvas (2006). Snow modeling resolution is set to 100 m in this study following consideration of data availability and required computational efforts.

4. Model calibration and validation

MM5 and the WEHY snow model were validated over the three study watersheds before projecting the snow regime in the 21st century. For validation, a reanalysis dataset was utilized as the forcing data of the MM5, instead of GCM control runs or future climate projection realizations, so as to be able to obtain time series comparable to the corresponding observations. Although a reanalysis is also a GGM output, it is synthesized to various observation data by means of data assimilation, and is frequently used as an alternative to observation data. The National Center for Atmospheric Research/National Centers for Environmental Prediction (NCAR/NCEP) Reanalysis I dataset was employed. Based on the NCAR/NCEP Reanalysis I dataset, the MM5 was validated by comparing the simulated precipitation with the corresponding observations over the three study watersheds, and the validation results were presented in a previous study (Ishida et al., 2015a).

The atmospheric data obtained by the validated MM5 were used to calibrate and validate the WEHY snow model over the three study watersheds. The main objective of this study is to analyze future climate impacts on snow distribution. Therefore, the selected model should be capable of reasonably simulating the snow regime throughout the study watersheds. To assess such model capability, the WEHY snow model was calibrated by comparing the simulated snow water equivalent with the corresponding observations at select gauging observation stations over the study watersheds. In the calibration, the time constant for albedo, converged value of albedo, and maximum albedo, which are parameters that account for the reflectance of snow (Ohara and Kavvas, 2006), were adjusted by trial-and-error. After the calibration, the snow model was validated at all the available gauging stations within the three study watersheds using the calibrated model parameters. Most gauging observation data are available after 1999. Thus 14 water years, from October 1999 through September 2013, were utilized for the model calibration and validation.

Calibration was performed utilizing one gauging station within each watershed: CAP within the ARW, GOL within the YRW, and BKL within the FRW. The three gauging stations are spatially distributed and have sufficient observation data during the calibration period. The first three water years of the selected observation data period (wy2000–wy2002) were utilized for the calibration. Table 2 shows the daily mean and standard deviation of the simulated and the observed snow water equivalent, and the correlation coefficient and the Nash-Sutcliffe coefficient at the three selected observation locations during the calibration period. The simulated snow water equivalent and the gauging observation data at the three selected stations during the calibration period were plotted in the shaded area of the plots in Fig. 3. There are large differences between the daily mean simulated snow water equivalent and the observation data at GOL and BKL despite the appearance of agreement in the plots. This inconsistency is a result of missing observation data which is difficult to visualize in the plots, especially during no-snow periods. As a result, the correlation coefficient and the Nash-Sutcliffe coefficient were utilized for the model calibration after excluding the missing periods of the observation data from the corresponding calculations. The correlation coefficient is 0.920 at CAP, 0.976 at GOL, and 0.964 at BKL during the three water years (wy2000–wy2002). The Nash-Sutcliffe coefficient is 0.700 at CAP, 0.952 at GOL, and 0.928 at BKL. The simulated snow water equivalent is in very good agreement with the observation data at GOL and BKL. The correlation coefficient and the Nash-Sutcliffe coefficient are sufficiently high at CAP, despite the simulated results slightly overestimating the snow water equivalent.

Table 2
Statistics between the simulated hourly snow water equivalent and the corresponding observations at the three gauging stations (CAP, GOL, and BKL) during three water years (wy2000–wy2002) for the model calibration.

Station		CAP	GOL	BKL
Watershed		ARW	YRW	FRW
Observation	Mean (m)	0.22	0.36	0.58
	STD (m)	0.23	0.36	0.41
Simulation	Mean (m)	0.23	0.29	0.34
	STD (m)	0.27	0.34	0.42
Correlation coefficient		0.920	0.976	0.964
Nash-Sutcliffe coefficient		0.700	0.952	0.928

Utilizing the calibrated model parameters, the snow model simulation was performed for 14 water years (wy2000-wy2013) over the three study watersheds. The simulated snow water equivalent is illustrated together with the corresponding observations in Fig. 3. Daily mean, standard deviation, correlation coefficient, and the Nash-Sutcliffe coefficient were calculated at all the available gauging stations: eight stations within the ARW, three stations within the YRW, and five stations within the FRW (See Table 3). The calibration period was excluded from the computations at the three stations (CAP, GOL and BKL) used for the calibration. Correlation coefficient is >0.8, and the Nash-Sutcliffe coefficient is >0.6 at all the stations. In this study, the snow model did not use observed precipitation and air temperature, but rather used atmospheric inputs that were simulated by the MM5. Nevertheless, these coefficients show good agreement between the simulated snow water equivalent and the corresponding observations at all the available gauging stations within the three study watersheds.

5. Climate change impacts on snow distribution

Snow regime was simulated over the three study watersheds during the 90-water year future period (wy2010–2100) by means of the WEHY snow model, utilizing the calibrated and validated model parameters, based on 13 future climate projection realizations. For analysis, the ensemble average of the snow water equivalent over all of the 13 realizations was calculated at each 100 m model grid within the three study watersheds for each month. In addition, the ensemble averages of the snow water equivalent over four A1B realizations, four A2 realizations, and four B1 realizations were calculated. There is only one realization for the A1FI scenario from CCSM3, allowing only one A1FI realization result to be compared with the ensemble averages over the realizations in the other scenarios. After calculating the above ensemble averages, the 30-year average was calculated for each ensemble average including the single A1FI realization for three separate periods; the early 21st century (wy2010–2040), the middle 21st century (wy2040–2070), and the late 21st century (wy2070–2100). The study watersheds were then divided into five elevation ranges: 0–1200 m, 1200–1600 m, 1600–2000 m, 2000–2400 m, 2400–2800 m, and 2800–3200 m. The snow covered areas and the snow water equivalent during these three periods were examined for the five divided elevation ranges as well as for the entire area of the three study watersheds. Meanwhile, the slope of the trend

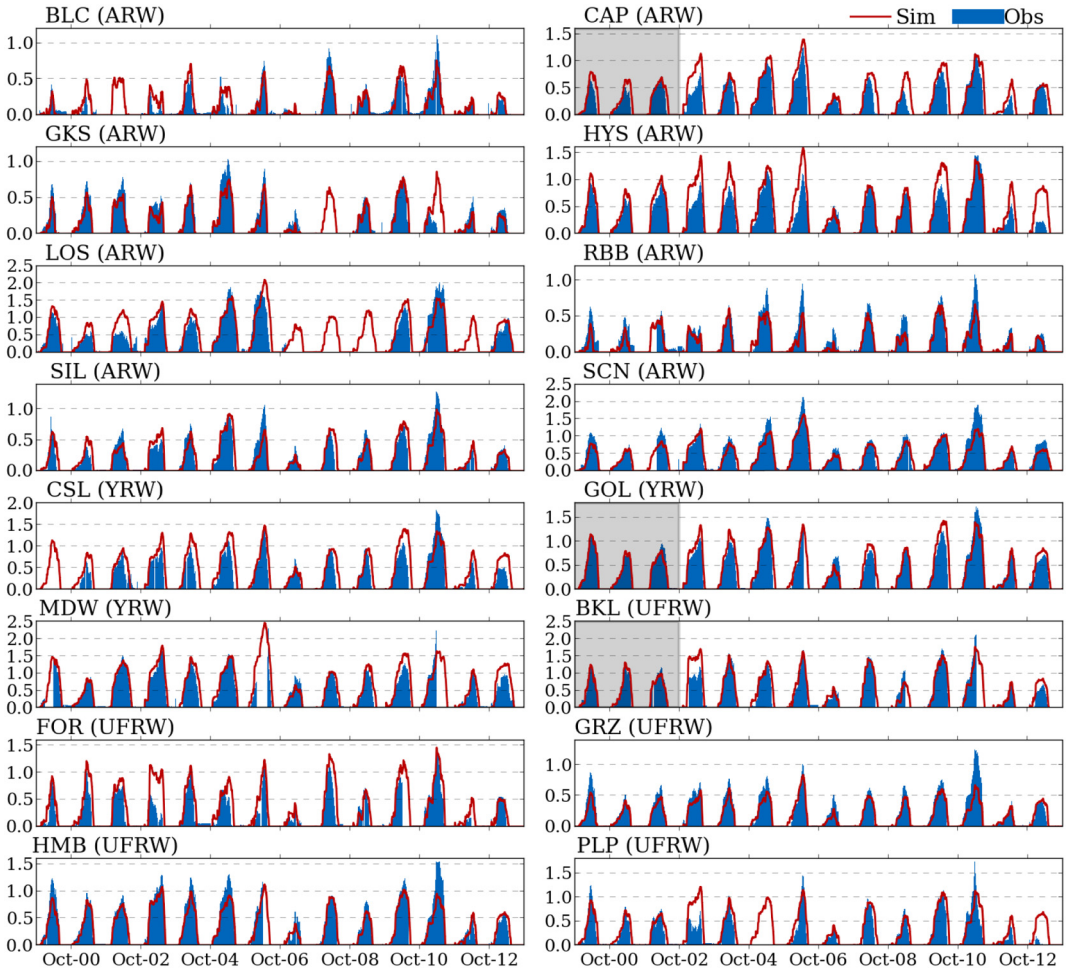

Fig. 3. Comparison of hourly snow water equivalent between the simulated results and the corresponding observations at the gauging stations during 14 years (wy2000–wy2013). The calibration period for the three stations (CAP, GOL, and BKL) is shaded.

line for snow water equivalent in each month throughout the 21st century was calculated, at each 100 m model grid and for each of the ensemble averages, by means of the Theil-Sen estimator. The unit of the slope was converted to percentage by dividing the slope in meter by the snow water equivalent at the water year 2010 on the trend line. To avoid dividing by a very small value, the slope in percentage was set at 0% when the snow water equivalent at the water year 2010 on the trend line was <5 mm. In addition, the Mann-Kendall trend test, which is a non-parametric statistical test on the significance of time series trends, was applied to snow water equivalent in each month to detect any existing trend in snow water equivalent at each model grid within the study watersheds during the 21st century.

Fig. 4 shows the 30-year ensemble averages of the snow water equivalent over the 13 realizations at each model simulation grid in January (snow accumulation period), March (snow peak period), and May (snow melt period) during the early 21st century (wy2010–wy2040),

Table 3
Statistics between the simulated hourly snow water equivalent and the corresponding observations at gauging stations during 14 years (wy2000–wy2013) for model validation. The calibration period (wy2000–2002) was excluded for the three stations that were used for the calibration (CAP, GOL, and BKL).

Station		CAP	BLC	GKS	HYS	LOS	RBB	SCN	SIL
Watershed		ARW	ARW	ARW	ARW	ARW	ARW	ARW	ARW
Observation	Mean (m)	0.35	0.07	0.20	0.33	0.61	0.19	0.46	0.27
	STD (m)	0.31	0.10	0.25	0.35	0.49	0.24	0.48	0.28
Simulation	Mean (m)	0.31	0.11	0.25	0.36	0.67	0.10	0.34	0.18
	STD (m)	0.36	0.18	0.20	0.42	0.69	0.16	0.38	0.24
Correlation coefficient		0.898	0.831	0.894	0.913	0.866	0.919	0.949	0.896
Nash-Sutcliffe coefficient		0.610	0.706	0.762	0.603	0.716	0.744	0.861	0.801
Station		GOL	CSL	MDW	BKL	FOR	GRZ	HMB	PLP
Watershed		YRW	YRW	YRW	FRW	FRW	FRW	FRW	FRW
Observation	Mean (m)	0.41	0.35	0.53	0.44	0.23	0.25	0.36	0.29
	STD (m)	0.43	0.40	0.47	0.51	0.31	0.28	0.41	0.35
Simulation	Mean (m)	0.36	0.36	0.52	0.40	0.27	0.15	0.26	0.27
	STD (m)	0.43	0.42	0.57	0.52	0.38	0.19	0.32	0.34
Correlation coefficient		0.944	0.874	0.935	0.930	0.898	0.931	0.959	0.863
Nash-Sutcliffe coefficient		0.876	0.664	0.813	0.855	0.606	0.784	0.874	0.686

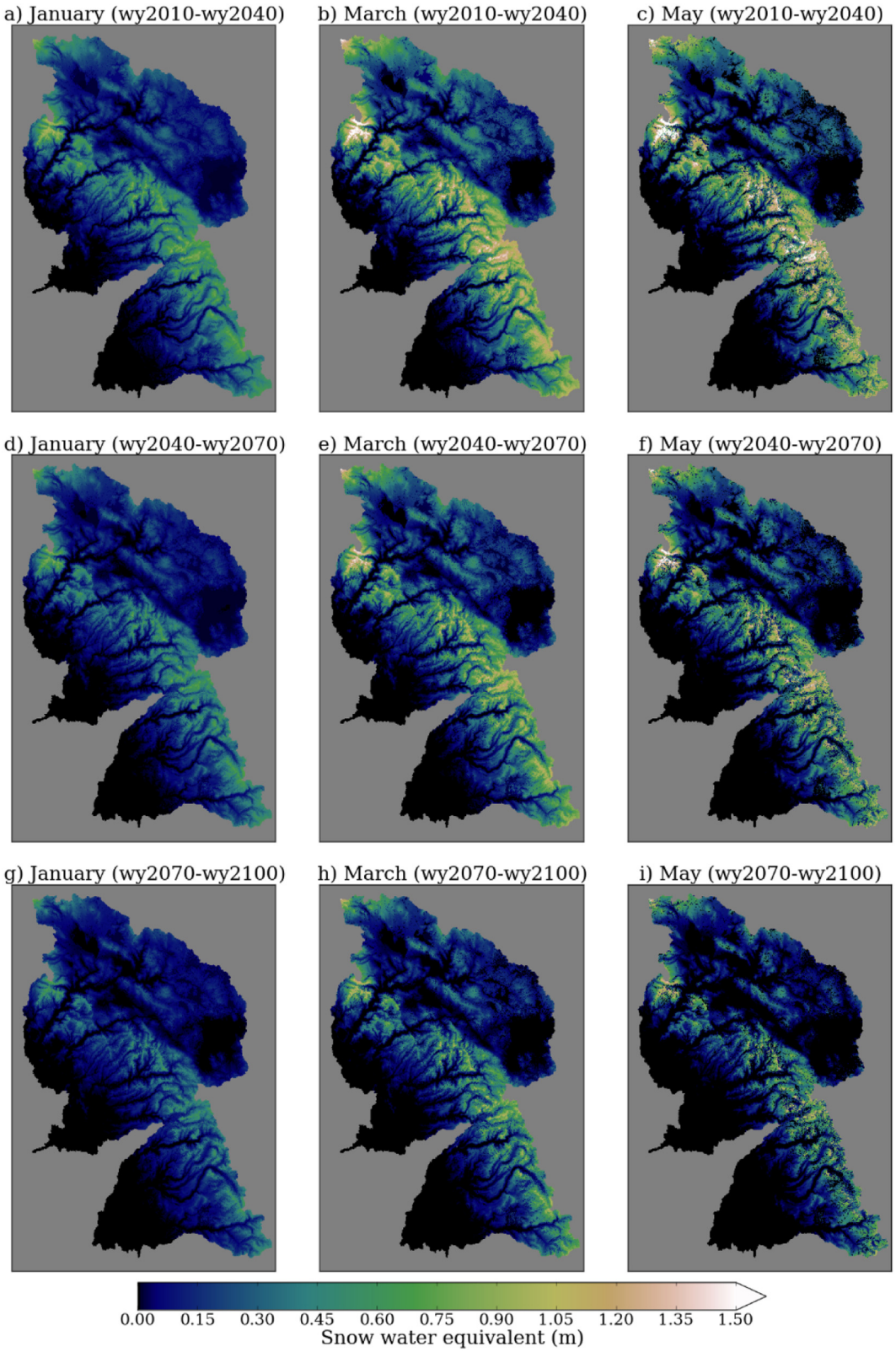

Fig. 4. Distribution of 30-year ensemble average snow water equivalent values for the 13 downscaled climate projection realizations in (left) January, (middle) March, and (right) May during (top) the early (wy2010–wy2040), (middle) the middle (wy2040–2070), and (bottom) the late 21st century (wy2070–wy2100).

the middle 21st century (wy2040–2070), and the late 21st century (wy2070–wy2100). The snow projection results indicate clearly that the snowpack will decrease over the study watersheds in the future. Percentages of snow covered areas over the entirety of the three study watersheds and over the five divided elevation ranges are shown in Fig. 5. During the early 21st century (wy2010–wy2040), on average, 85.5%, 80.3%, and 65.5% of the entirety of the three study watersheds is covered by snow in January, March, and May, respectively. The snow covered area of the three watersheds depends mainly on the air temperature in each month. The snow covered area will reduce by

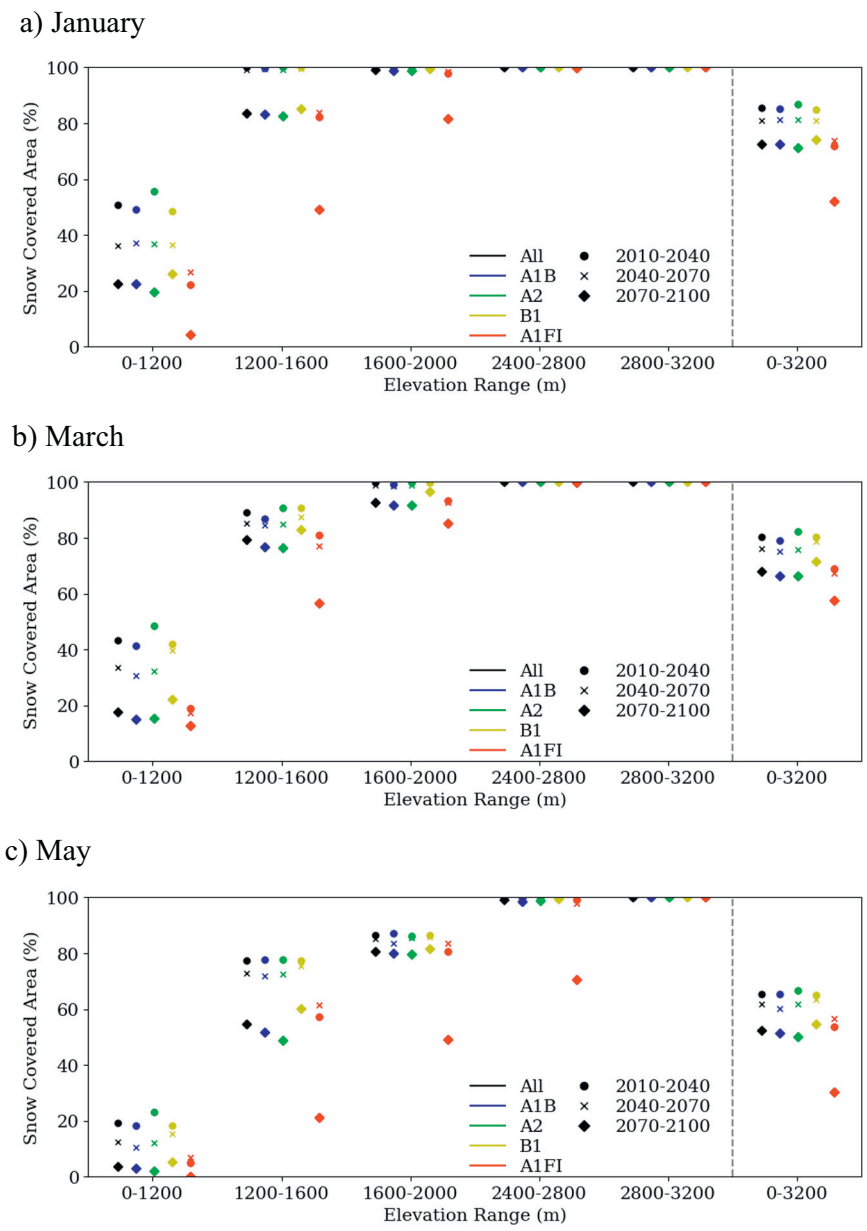

Fig. 5. Snow covered area of the simulated 30-year averaged snow conditions for each ensemble (All, A1B, A1FI, A2, and B1) over the five divided elevation ranges and the entire watersheds in (top) January, (middle) March, and (bottom) May during the early (wy2010–wy2040), the middle (wy2040–2070), and the late 21st century (wy2070–wy2100).

about 4.1% (4.5% for January, 4.1% for March, and 3.7% for May) during the middle 21st century and by about 12.7% (13% for January, 12.2% for March, 13% for May) during the late 21st century when compared to that during the early 21st century. As depicted in Fig. 5, almost all the reductions in the snow covered area between the early and the middle 21st century will occur at elevations between 0 m and 1600 m in January. Some reduction in the snow covered area will happen at elevations between 1600 m and 2000 m in March and May.

Reductions in the total amount of snow water equivalent over the entire three study watersheds are more severe when compared to the snow covered areas, as shown in Fig. 6. The 30-year average snow water equivalent in January will decrease by 28.0% in the middle 21st century and by 51.2% in the late 21st century, compared to that in the early 21st century. In March, the snow water equivalent will reduce by 25.3% and 51.3% in the middle and the late 21st century, respectively. The reduction in the total snow water equivalent is most severe in May with snow water equivalent decreasing by 29.4% during the middle 21st century and 57.3% during the late 21st century when compared to the early 21st century. Unlike the snow covered area, reductions in the snow water equivalent are contributed ~~to~~ by the entire area of the watersheds (Fig. 6). For instance, the magnitude of the reductions in the snow water equivalent will be the largest between 2400 m and 2800 m among the five divided elevation ranges in all of the three months. The reductions between the early and the late 21st century will be 12.1 cm, 18.2 cm, and 33.0 cm in January, March, and May, respectively.

The slope of the trend line in percentage and the *p*-value of the Mann-Kendall trend test for the ensemble average of snow water equivalent over the 13 realizations at each model grid in January, March, and May during the entire 21st century (wy2010–wy2100) are illustrated in Fig. 7. The snowpack will decrease during the 21st century throughout the three study watersheds through the snow accumulation and melting periods. The slope of the trend line for snow water equivalent is milder in higher elevation areas. In areas where the slope of the trend line is steep, snow will disappear in the late 21st century, as shown in Fig. 4. The slope of the trend line is also relatively mild on south-facing

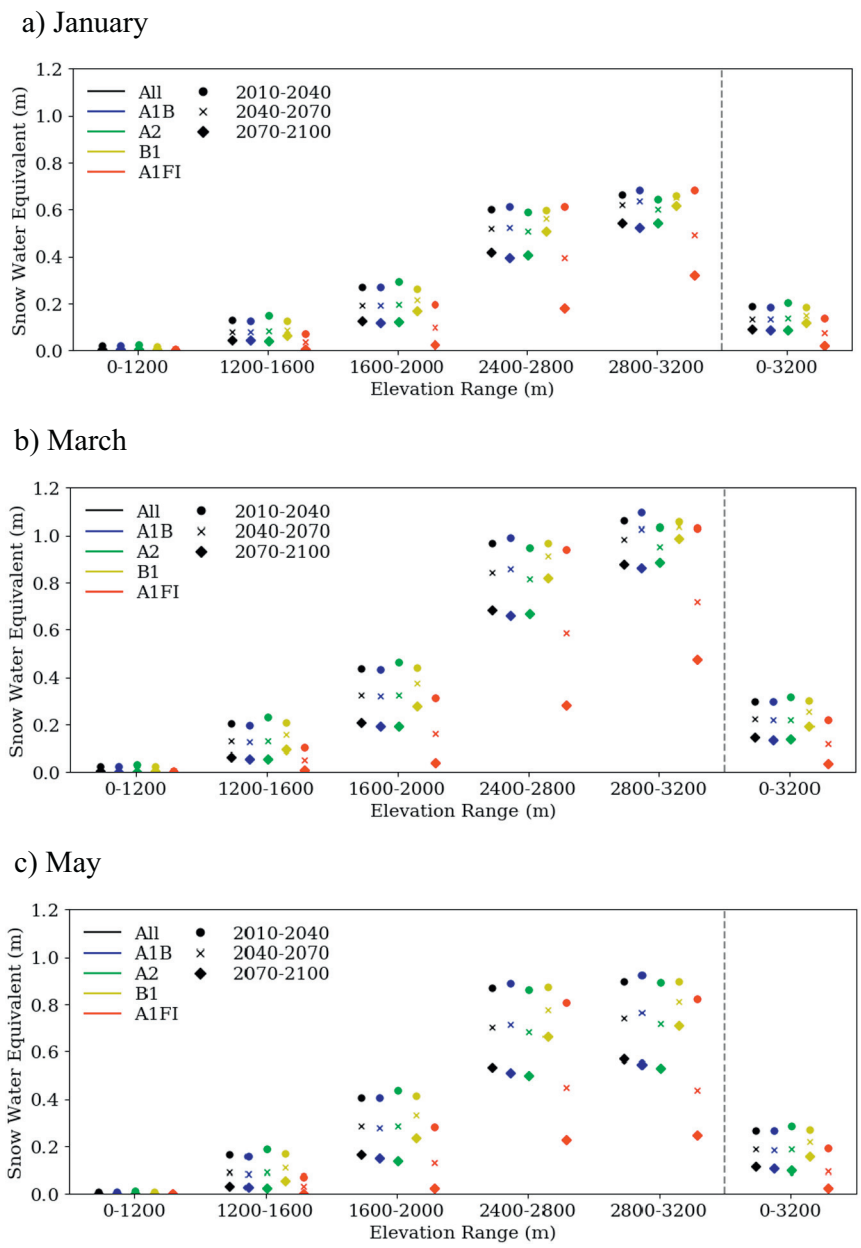

Fig. 6. Spatial average of 30-year ensemble average snow water equivalent values for all the 13 downscaled climate projection realizations and for A1B, A1FI, A2, and B1 scenarios over the five divided elevation ranges and the entire watersheds in (top) January, (middle) March, and (bottom) May during the early (wy2010–wy2040), the middle (wy2040–2070), and the late 21st century (wy2070–wy2100).

slopes. According to the Mann-Kendall trend test the downward trend in the snow water equivalent during January, March, and May is significant at the 99% confidence level throughout the three study watersheds, except in areas where there is little or no snow at the beginning of the 21st century.

Figs. 8–10 illustrate the 30-year ensemble average of snow water equivalent for each scenario during January, March, and May during the early 21st century (wy2010–wy2040), the middle 21st century (wy2040–2070), and the late 21st century (wy2070–wy2100). As plotted in Fig. 5, 85.1%, 71.8%, 86.9%, and 84.8% of the three study watersheds are covered by snow during the early 21st century (wy2010–wy2040) in January for the A1B, A1FI, A2, and B1 scenarios, respectively. Also in January, snow covered areas of the study watersheds account for 81.4%, 73.8%, 81.2%, and 81.1% for the A1B, A1F1, A2 and B1 scenarios, respectively, in the middle 21st century (wy2040–2070), and 72.4%, 52.2%, 71.3%, and 74.1%, respectively, in the late 21st century (wy2070–wy2100). The snow covered area in total is similar between A1B and A2 scenarios during all three future periods although the snow covered area of the A2 scenario is slightly larger than that for the A1B scenario in the lower elevations during the early 21st century. The snow covered area of the study watersheds for B1 scenario will gradually decrease in the future, but the reduction in B1 scenario is slightly milder through the future period when compared to A1B and A2 scenarios. The reduction in the snow covered area of the study watersheds is mainly due to the reductions at the low elevation areas between 0 m and 1600 m in January for A1B, A2, and B1 scenarios. For A1FI scenario, the snow covered area is smaller than that in the other scenarios in all periods. For January, the reduction in the snow covered area of the study watersheds between the middle and the late 21st century is approximately 20% for A1FI, while it is approximately 10% in the other scenarios.

In March, the snow covered areas of the three study watersheds are 79.0%, 69.1%, 82.3%, and 80.5% for the A1B, A1FI, A2, and B1 scenarios, respectively, during the early 21st century. They gradually reduce to

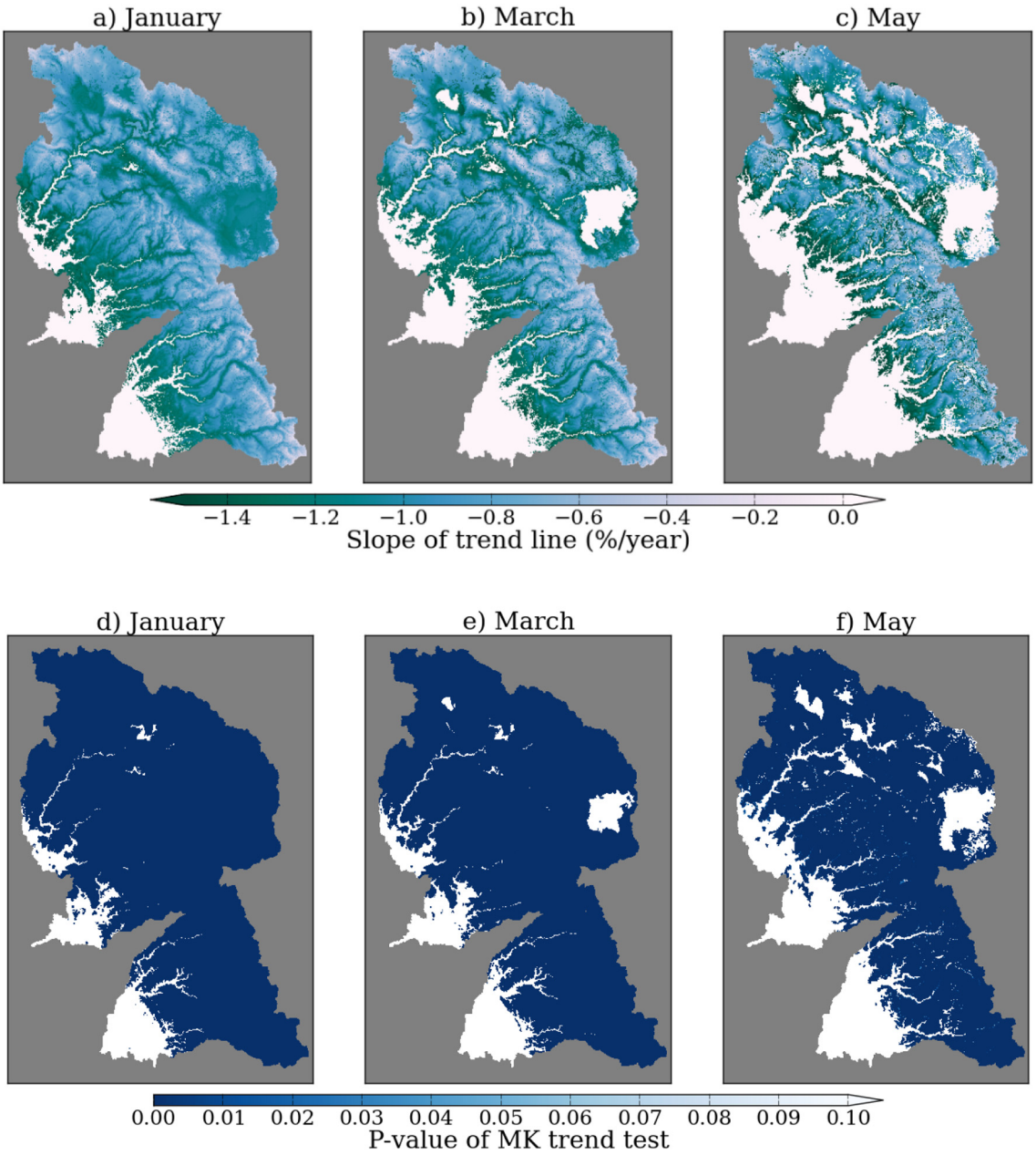
a) January
b) March
c) May
−1.4 −1.2 −1.0 −0.8 −0.6 −0.4 −0.2 0.0
Slope of trend line (%/year)
d) January
e) March
f) May
0.00 0.01 0.02 0.03 0.04 0.05 0.06 0.07 0.08 0.09 0.10
P-value of MK trend test

Fig. 7. (top) Slope of the trend line in percent and (bottom) *p*-value of the Mann-Kendall trend test with respect to the ensemble average snow water equivalent over the 13 downscaled climate projection realizations at each grid within the three study watersheds in (left) January, (middle) March, and (right) May during the 21st century (wy2010–wy2100).

75.0%, 67.3%, 75.7%, and 78.8%, respectively, in the middle 21st century, and 66.2%, 57.5%, 66.3%, and 71.5%, respectively, in the late 21st century. Although the snow covered area in March is generally smaller than that in January, the differences among the scenarios and among the periods are similar over all elevation ranges between January and March. Only for the most severe scenario, A1F1, is the reduction in the snow covered area of the three study watersheds between the early and the late periods smaller in March (11.5%) compared to that in January (19.6%).

In May, the snow covered areas of the three study watersheds for the A1B, A1FI, A2, and B1 scenarios are 65.6%, 53.7%, 66.6%, and 65.1%, respectively, in the early 21st century, 60.3%, 56.5%, 61.8%, and 63.6%, respectively, in the middle 21st century, and then 51.4%, 30.4%, 50.1%, and 54.8%, respectively, in the late 21st century. The differences in the snow covered areas in May are also similar to those in January at all elevation ranges among the periods and among the scenarios, except for A1FI scenario. For A1FI scenario, the reduction at the elevations between 0 m and 1200 m is almost the same between March and May. However, the reduction in May is larger than that in March at elevations between 1200 m and 2800 m, and at elevations between 2400 m and 2800 m, the snow covered area reduces by 28.6% in May while there is no reduction in the snow covered area in March. In addition, the snow covered area in May is much smaller than that in January. Consequently, the snow coverage area of the three study watersheds for A1FI scenario reduces to approximately 30% in the late 21st century.

The snowpack volume shows clear reductions through the future period as shown in Fig. 6. Compared to the early 21st century, the 30-year average snow water equivalent over the three study watersheds in January decreases by 28.0%, 45.9%, 33.1%, and 18.9% in the middle 21st century; and by 53.8%, 83.5%, 57.8%, and 35.1% in the late 21st century, for A1B, A1FI, A2, and B1 scenarios, respectively. In March, the percentage reductions in the 30-year average snow water equivalent over the three study watersheds for A1B, A1FI, A2, and B1 scenarios are 26.2%, 46.4%, 30.5%, and 15.1%, respectively, in the middle 21st century; and 54.5%, 83.2%, 56.9%, and 36.5%, respectively, in the late 21st century.

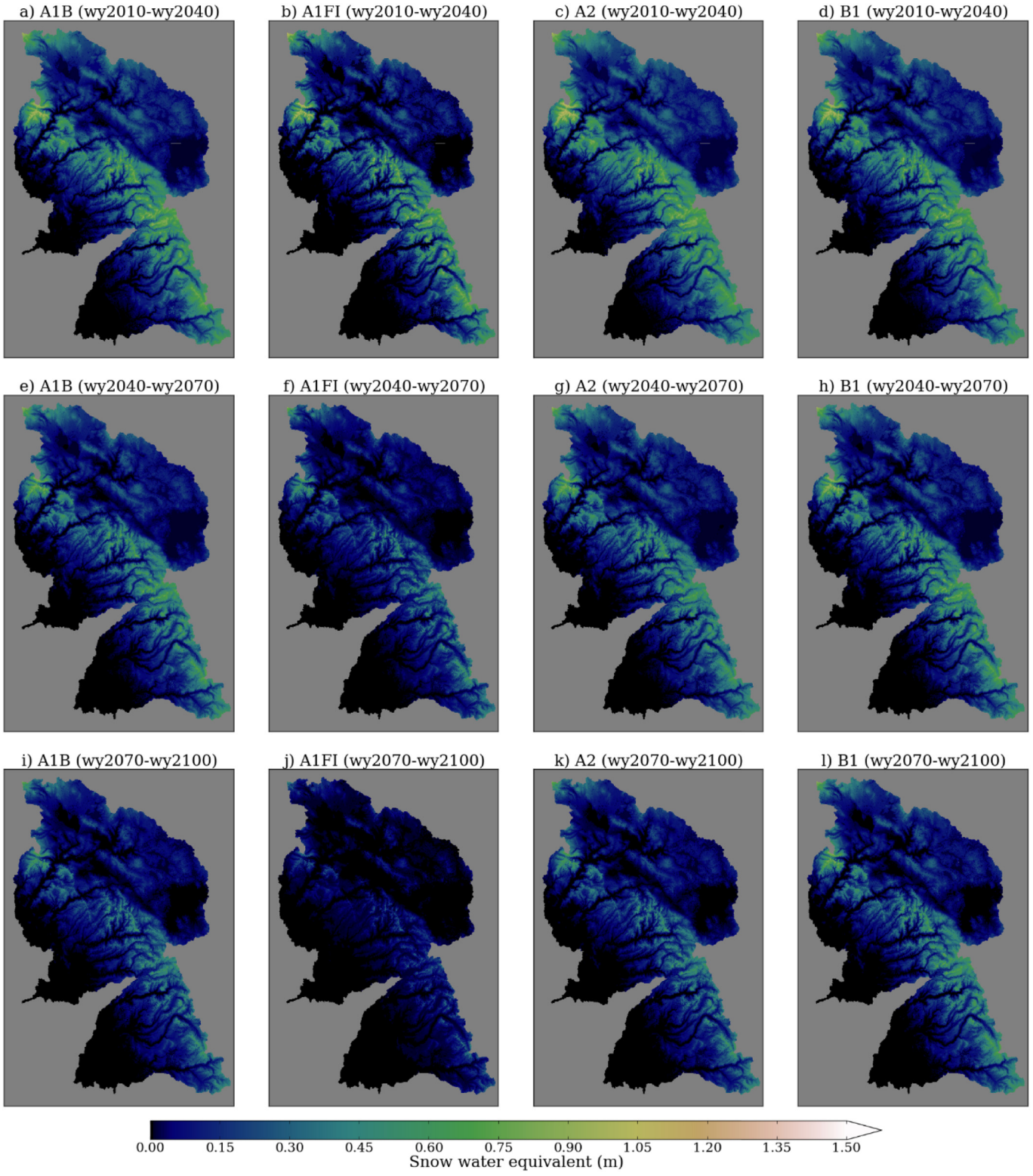

Fig. 8. Distributions of 30-year ensemble average snow water equivalent for A1B, A1FI, A2, and B1 scenarios (from left to right) in January during (top) the early (wy2010–wy2040), (middle) the middle (wy2040–2070), and (bottom) the late 21st century (wy2070–wy2100).

Furthermore, those in May are 30.3%, 50.4%, 34.2%, and 19.8% respectively, in the middle 21st century; and then 60.1%, 86.0%, 64.7%, and 41.9%, respectively, in the late 21st century.

Reductions in snowpack volume (snow water equivalent) over the three study watersheds through the 21st century, in total, are similar for A1B and A2 scenarios, as was the case for the snow covered area. However, the reduction for A1B scenario is smaller at lower elevations than the reduction for A2 scenario. Conversely, the reduction for A1B scenario is larger at higher elevations in January and March. For B1 scenario, reductions in snow water equivalent are milder through the future period than for the A1B scenario despite B1 scenario projections having snow distributions similar to A1B during the early 21st century. In total, the absolute difference in snow water equivalent over the three study watersheds between A1B and B1 is only 1% in the early 21st

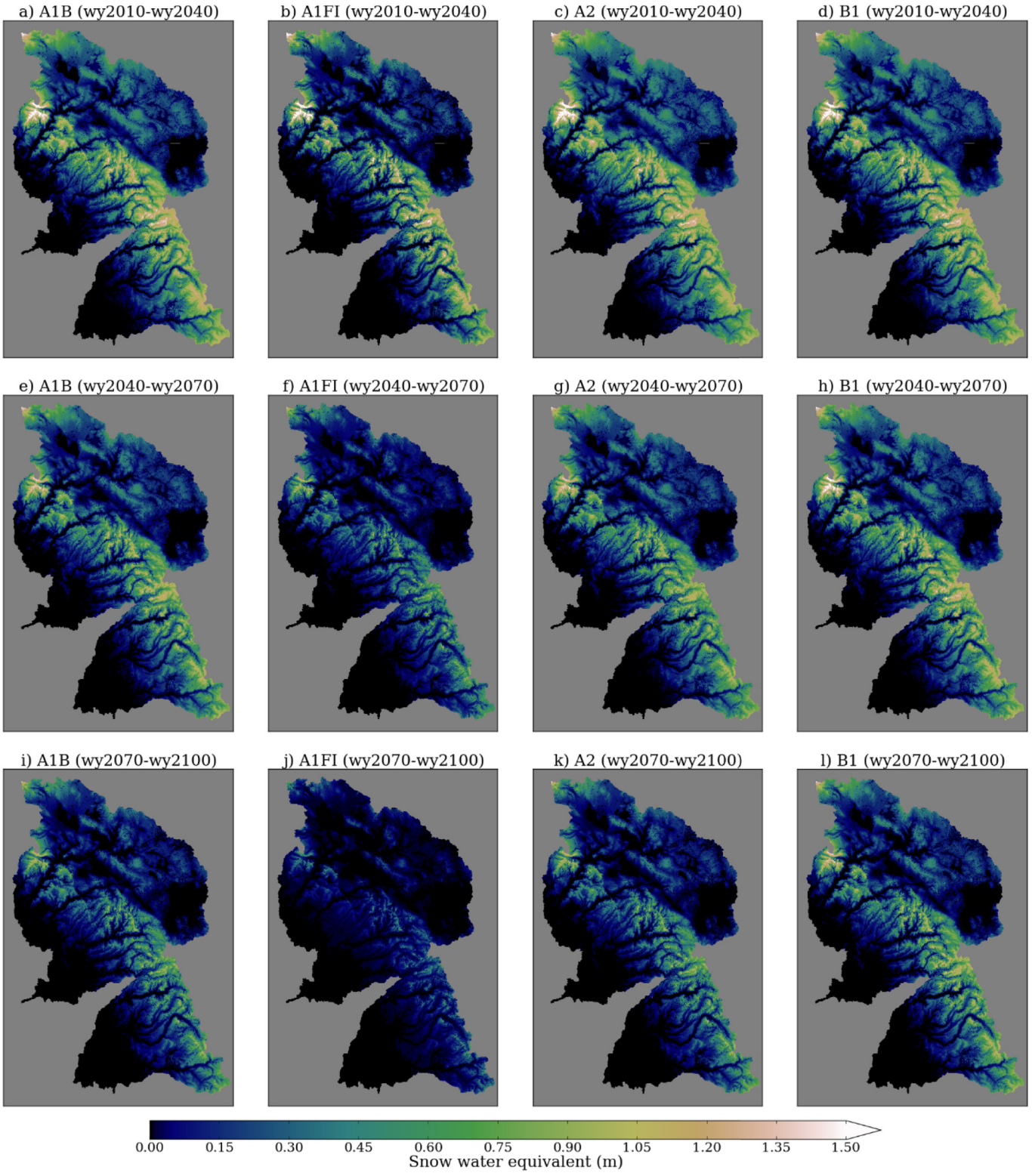

Fig. 9. Distributions of 30-year ensemble average snow water equivalent for A1B, A1FI, A2, and B1 scenarios (from left to right) in March during (top) the early (wy2010–wy2040), (middle) the middle (wy2040–2070), and (bottom) the late 21st century (wy2070–wy2100).

century, while it is 16.3% and 41.0% in the middle and late 21st century, respectively. Thus the differences in snowpack between A1B and B1 scenarios gradually increase toward the future. For A1FI scenario, almost half of the snowpack will disappear in the middle 21st century, and <17% of the snow water equivalent will remain in the late 21st century. Compared to the other scenarios, A1FI scenario projects much less snowpack over the three study watersheds throughout the 21st century in all three months. Even in the early 21st century, the snow water equivalent over the three study watersheds for A1FI scenario is 25–30% smaller than that for A1B scenario. In the late 21st century,

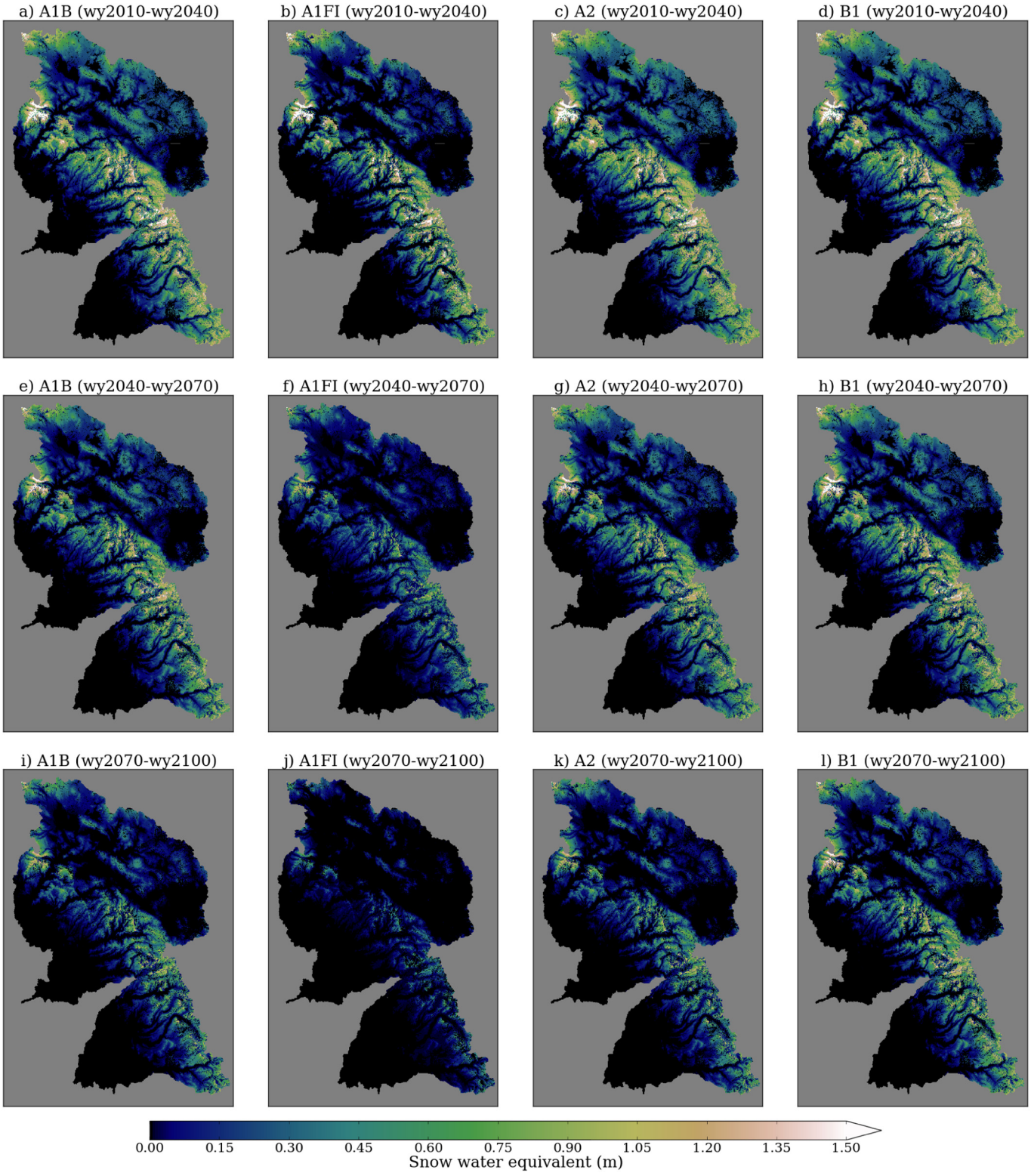

Fig. 10. Distributions of 30-year ensemble average snow water equivalent for A1B, A1FI, A2, and B1 scenarios (from left to right) in May during (top) the early (wy2010–wy2040), (middle) the middle (wy2040–2070), and (bottom) the late 21st century (wy2070–wy2100).

the snow water equivalent for A1FI scenario is 73–75% smaller than that for A1B scenario. While the difference of the snow water equivalent between A1B and A1FI is 38–57% at elevations between 2400 m and 3200 m, it is 79–89% at elevations between 1200 m and 2400 m.

Fig. 11 illustrates the slope of the trend line in percentage by the Theil-Sen estimator with respect to the ensemble average of snow water equivalent over the A1B, A1FI, A2, and B1 scenarios at each grid within the three study watersheds during the three months (January, March, and May) through the 21st century (wy2010–wy2100). All the scenarios project that the snowpack in all three months will decrease over almost the entire snow covered areas of the three study watersheds during the 21st century. According to

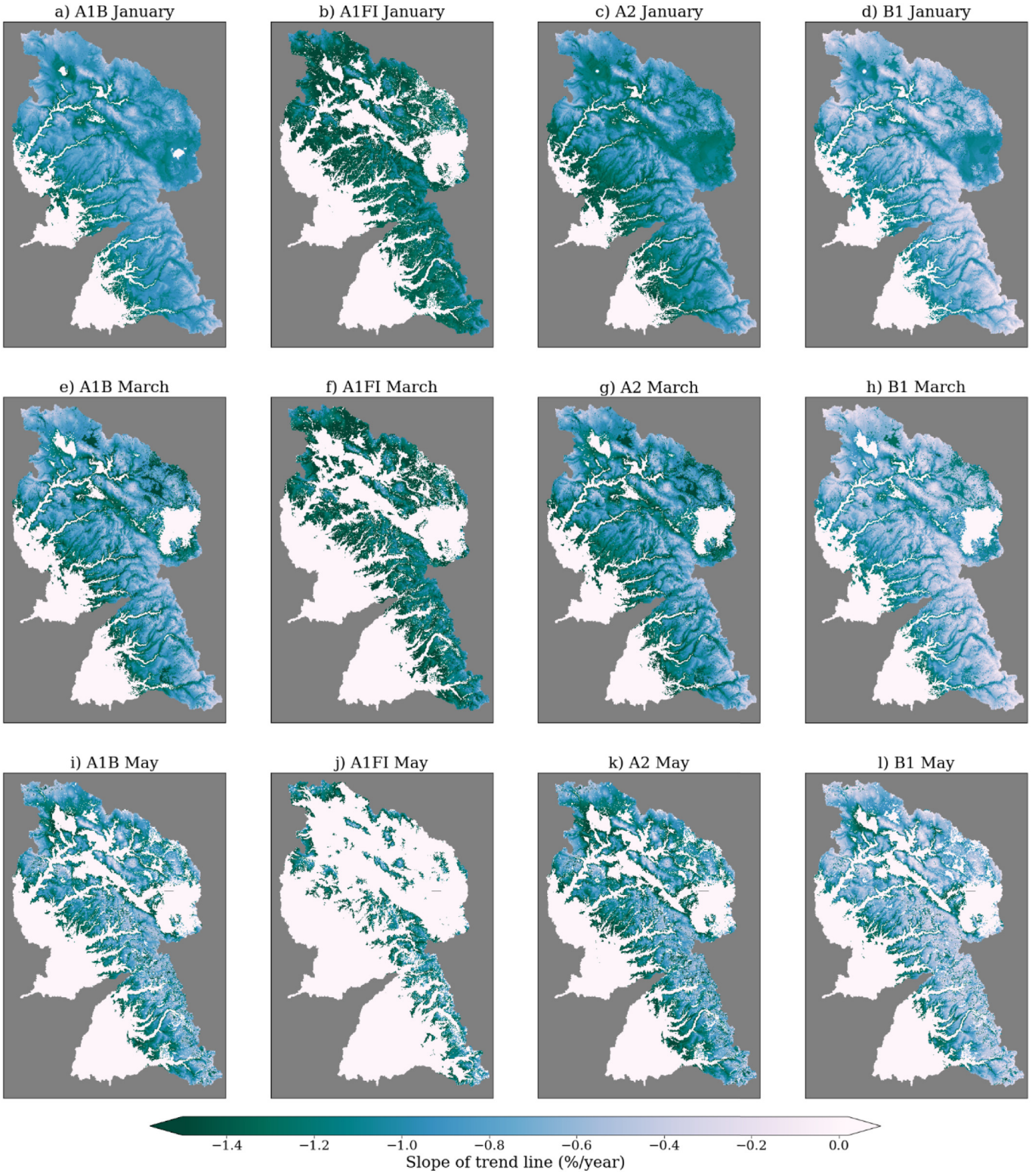

Fig. 11. Slope of the trend line in percent with respect to the ensemble average snow water equivalent for the A1B, A1FI, A2, and B1 scenarios at each grid within the three study watersheds in (top) January, (middle) March, and (bottom) May during the 21st century (wy2010–wy2100).

the Mann-Kendall trend test for the 90-year period (wy2010–2100), the downward trend is significant at the 99% confidence level for almost the entire snow covered areas as shown in Fig. 12. Only at high elevation ridges in B1 scenario is a significant downward trend not detected, although it is difficult to differentiate those areas in Fig. 12. To clearly show the areas with no trend for B1 scenario, the Mann-Kendall trend test was additionally applied for the time periods ranging from 20 years (wy2010–2030) to 90 years (wy2010–2100), which start from water year 2010. The shortest time interval among the time periods for which the significant downward trend at the 99% confidence level was detected is plotted at each simulation grid for January, March, and May in Fig. 13. This

Fig. 12. *P*-value of the Mann-Kendall trend test with respect to the ensemble average snow water equivalent for the A1B, A1FI, A2, and B1 scenarios at each grid within the three study watersheds in (top) January, (middle) March, and (bottom) May during the 21st century (wy2010–wy2100).

distribution plot of the shortest time intervals shows that, for B1 scenario, reduction in snowpack at higher elevations requires longer to become significant. There are some areas at high elevation ridges where it takes >90 years for the reduction in snowpack to become significant, or where snowpack will not decrease in the future.

6. Discussion

The snow regime projections show significant downward trends over the three watersheds in California in the 21st century for each of the four SRES scenarios (A1B, A1FI, A2, and B1), and for the ensemble

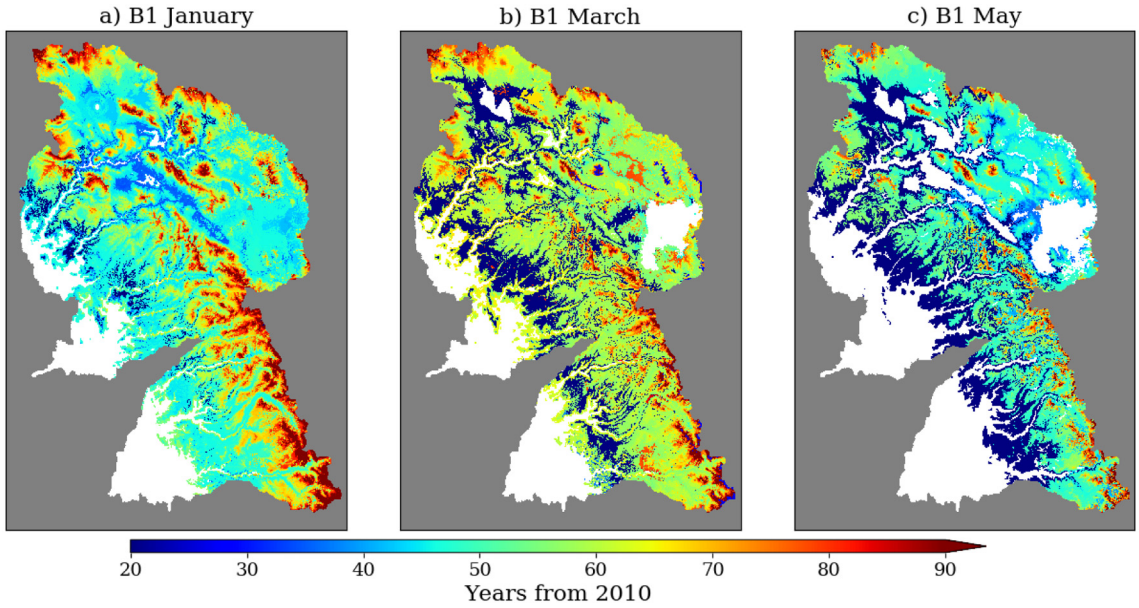

Fig. 13. The shortest time interval among the time periods (20–90 years from 2010) for which the significant downward trend at the 99% confidence level was detected for B1 scenario.

average over the 13 downscaled future climate projections. The significant downward trends were found in January, March, and May, indicating that the snowpack will decrease during the snow accumulation (January), peak (March), and melting (May) periods during the 21st century.

Snowpack reduction in the 21st century is different among the months and among the scenarios. For instance, the ensemble average results over the 13 future climate projections show that the reduction in the snowpack amount (snow water equivalent) through the 21st century is similar between the snow accumulation period (January) and the snow peak period (March), but is larger in the snow melting period (May) than in the other periods, as shown in Fig. 7a–c. These results indicate that warmer air temperature after the snow peak period (March) affects the snowpack reduction at higher elevations through the 21st century. The relationship between air temperature and snow melt is non-linear. Because the snow regime projections in this study were conducted at 100 m grid resolution at hourly time intervals by a physically-based snow model, there is no certain threshold of air temperature where snow starts to melt, and the snow condition changes at each grid at every hour during the model simulations. Despite this, it is still important to investigate the relationship between change in snow regime and air temperature rise in the future, at a coarser spatial and temporal scale, although the relationship may not always be explicit. Fig. 14 shows the differences in the 30-year ensemble average of the area-average monthly mean air temperature between the early (wy2010–wy2040) and the middle (wy2040–2070), and between the

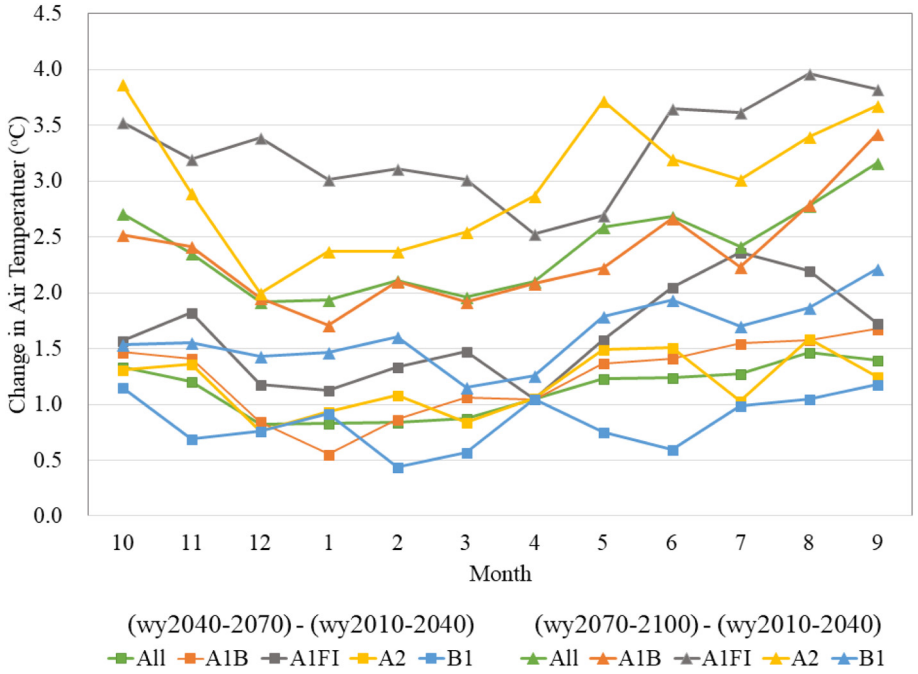

Fig. 14. Difference in 30-year ensemble average of area-averaged monthly mean air temperature over the three study watersheds between the early (wy2010–wy2040) and the middle (wy2040–2070), and between the early (wy2010–wy2040) and the late 21st century (wy2070–wy2100).

early (wy2010–wy2040) and the late 21st century (wy2070–wy2100). With respect to the ensemble average air temperature over the 13 projections, increases in air temperature in April and May are larger than those from December through March. This difference may contribute to the larger reduction in snowpack in May. Similar results can be found for all the scenarios' ensemble average results. Furthermore, increase in air temperature is almost always smaller for B1 scenario than for the other scenarios, and conversely it is larger for A1FI scenario. These results are consistent with the reductions in snowpack amount.

Among the four future climate scenarios, A1B and A2 project the snow regime over the three study watersheds during the 21st century similar to each other despite A2 being a more severe scenario than A1B. The air temperature is slightly lower for the A2 scenario than that for the A1B scenario during the early 21st century. As shown in Fig. 14, however, the difference in air temperature between the early and the late 21st century is larger for A2 scenario than that for A1B scenario. These results may explain why A2 becomes a more severe scenario than A1B. The snow regime projections for A1FI and B1 scenarios are clearly different from those of A1B and A2. Increase in air temperature is almost always smaller for B1 scenario than that for the other scenarios, and conversely it is larger for A1FI scenario. Consequently, while A1FI scenario projects the least snowpack, B1 scenario projects more snowpack through the 21st century when compared to A1B and A2 scenarios.

The slope of the trend line of the snow water equivalent is negative over almost the entire snow covered area through the snow accumulation to melting periods in the B1 scenario (Fig. 11). Snow reduction is not significant at some high elevation ridges in the three watersheds (Fig. 13). The "non-significant reduction" area is largest in January, implying that the global warming will not affect snow/rainfall ratio in those high elevation ridges in the B1 scenario, although it will affect the snow melting process. The other three scenarios (A1B, A1FI, and A2) project a significant downward trend in the snowpack over the entire snow covered areas of the three study watersheds during the 21st century, indicating that global warming effects will reach even the high mountainous peaks in these three scenarios.

7. Summary and conclusions

The impacts of climate change on the snow distribution through the 21st century were investigated over three mountainous watersheds in Northern California by means of a regional climate model (MM5) and a physically-based snow model (the WEHY snow model). Before projecting the future snow conditions, the snow model was calibrated by comparing the simulated results with the corresponding observation data at one selected gauging station per watershed. Then the snow model with the calibrated model parameters was validated by comparing the simulated results with the observation data at all the available gauging stations within the three study watersheds. The future climate conditions during a 90-year future period for water years 2010 to 2100 were obtained from 13 future climate projection realizations from two GCMs (ECHAM5 and CCSM3) based on four SRES scenarios (A1B, A1FI, A2, and B1). The 13 future climate projection realizations were dynamically downscaled at 9 km resolution by the MM5 regional atmospheric model. With the downscaled variables based on the 13 future climate projection realizations, snow distributions over the three study watersheds were projected by means of the WEHY snow model with the calibrated and validated model parameters, which includes further downscaling of the snow variables based on the elevation and the topographic aspect over the study watersheds. The ensemble average of the projected snow distribution was calculated over the 13 future climate projection realizations and each scenario. This study focused on the snow distribution during three months: January, March, and May, which represent snow accumulation, peak, and melting periods, respectively. Then, the climatology of the snow distribution was compared between three time slices, and the trends in the snow distribution were analyzed by means of the Theil-Sen estimator and the Mann-Kendall trend test.

The snow regime projection results show that the snowpack reduction through the 21st century is similar between the snow accumulation period (January) and the snow peak period (March), but it is larger during the snow melting period (May) than during the other periods. Snowpack reduction is larger at higher elevation areas during the snow melting period when compared to the other periods. Scenario comparisons show that A1B and A2 project the snow regime over the three study watersheds during the 21st century similarly, while B1 projects more snowpack and A1FI projects less snowpack compared to A1B and A2 scenarios. The downward trend in the snowpack is significant over all the watersheds for the three scenarios (A1B, A1FI, and A2). However, the snowpack reduction is not significant in some high elevation ridges for the B1 scenario.

References

Bavay, M., Lehning, M., Jonas, T., Löwe, H., 2009. Simulations of future snow cover and discharge in Alpine headwater catchments. Hydrol. Process. 23,95–108. https://doi.org/10.1002/hyp.7195.

Bilbao, R.A.F., Gregory, J.M., Bouttes, N., 2015. Analysis of the regional pattern of sea level change due to ocean dynamics and density change for 1993–2099 in observations and CMIP5 AOGCMs. Clim. Dyn. 45,2647–2666. https://doi.org/10.1007/s00382-015-2499-z.

Burnett, A.W., Kirby, M.E., Mullins, H.T., Patterson, W.P., 2003. Increasing Great Lake-effect snowfall during the twentieth century: a regional response to global warming? J. Clim. 16, 3535–3542.

California Department of Water Resources, 2003. California's Groundwater, Bulletin 118, Update 2003. California Department of Water Resources, p. 246.

Carson, M., Köhl, A., Stammer, D., A. Slangen Ab, Katsman Ca, W. Van De Wal Rs, Church J, White N., 2016. Coastal Sea level changes, observed and projected during the 20th and 21st century. Clim. Chang. 134,269–281. https://doi.org/10.1007/s10584-015-1520-1.

Castebrunet, H., Eckert, N., Giraud, G., Durand, Y., Morin, S., 2014. Projected changes of snow conditions and avalanche activity in a warming climate: the French Alps over the 2020–2050 and 2070–2100 periods. Cryosphere 8,1673–1697. https://doi.org/10.5194/tc-8-1673-2014.

Christensen, J.H., Christensen, O.B., 2007. A summary of the PRUDENCE model projections of changes in European climate by the end of this century. Clim. Chang. 81,7–30. https://doi.org/10.1007/s10584-006-9210-7.

Christensen, J.H., Carter, T.R., Rummukainen, M., Amanatidis, G., 2007. Evaluating the performance and utility of regional climate models: the PRUDENCE project. Clim. Chang. 81,1–6. https://doi.org/10.1007/s10584-006-9211-6.

Cline, D.W., 1997. Effect of seasonality of snow accumulation and melt on snow surface energy exchanges at a continental alpine site. J. Appl. Meteorol. 36, 32–51.

Colle, B.A., Mass, C.F., 2000. The 5–9 February 1996 flooding event over the Pacific northwest: sensitivity studies and evaluation of the MM5 precipitation forecasts. Mon. Weather Rev. 128,593–617. https://doi.org/10.1175/1520-0493(2000)128<0593:TFFEOT>2.0.CO;2.

Collins, W.D., Bitz, C.M., Blackmon, M.L., Bonan, G.B., Bretherton, C.S., Carton, J.A., Chang, P., Doney, S.C., Hack, J.J., Henderson, T.B., Kiehl, J.T., Large, W.G., McKenna, D.S., Santer, B.D., Smith, R.D., 2006. The community climate system model version 3 (CCSM3). J. Clim. 19,2122–2143. https://doi.org/10.1175/JCLI3761.1.

Daly, C., Neilson, R.P., Phillips, D.L., 1994. A statistical-topographic model for mapping climatological precipitation over mountainous terrain. J. Appl. Meteorol. 33,140–158. https://doi.org/10.1175/1520-0450(1994)033<0140:ASTMFM>2.0.CO;2.

Daly, C., Halbleib, M., Smith, J.I., Gibson, W.P., Doggett, M.K., Taylor, G.H., Curtis, J., Pasteris, P.P., 2008. Physiographically sensitive mapping of climatological temperature and precipitation across the conterminous United States. Int. J. Climatol. 28,2031–2064. https://doi.org/10.1002/joc.1688.

Dettinger, M.D., Cayan, D.R., Meyer, M.K., Jeton, A.E., 2004. Simulated hydrologic responses to climate variations and change in the Merced, Carson, and American River basins, Sierra Nevada, California, 1900–2099. Clim. Chang. 62,283–317. https://doi.org/10.1023/B:CLIM.0000013683.13346.4f.

Dettinger, M.D., Ralph, F.M., Das, T., Neiman, P.J., Cayan, D.R., 2011. Atmospheric rivers, floods and the water resources of California. Water 3,445–478. https://doi.org/10.3390/w3020445.

Dudhia, J., 1996. A multi-layer soil temperature model for MM5. Preprints, 6th PSU/NCAR Mesoscale Model Users' Workshop, NCAR, pp. 19–50.

Fischer, E.M., Knutti, R., 2014. Detection of spatially aggregated changes in temperature and precipitation extremes. Geophys. Res. Lett. 41,547–554. https://doi.org/10.1002/2013GL058499.

Flato, G., Marotzke, J., Abiodun, B., Braconnot, P., Chou, S.C., Collins, W., Cox, P., Driouech, F., Emori, S., Eyring, V., Forest, C., Gleckler, P., Guilyardi, E., Jakob, C., Kattsov, V., Reason, C., Rummukainen, M., 2013. Evaluation of Climate Models. Climate Change 2013: The Physical Science Basis. Contribution of Working Group I to the Fifth Assessment Report of the Intergovernmental Panel on Climate Change. pp. 741–866.

Garvert, M.F., Woods, C.P., Colle, B.A., Mass, C.F., Hobbs, P.V., Stoelinga, M.T., Wolfe, J.B., 2005. The 13–14 December 2001 IMPROVE-2 event. Part II: Comparisons of MM5

Model Simulations of Clouds and Precipitation with Observations. J. Atmos. Sci. 62,3520–3534. https://doi.org/10.1175/JAS3551.1.
Grell, G.A., Dudhia, J., Stauffer, D.R., 1994. A description of 5th generation Penn State/NCAR Meso-scale Model (MM5). NCAR Technical Note NCAR/TN-398+STR. NCAR.
Hayhoe, K., Cayan, D., Field, C.B., Frumhoff, P.C., Maurer, E.P., Miller, N.L., Moser, S.C., Schneider, S.H., Cahill, K.N., Cleland, E.E., Dale, L., Drapek, R., Hanemann, R.M., Kalkstein, L.S., Lenihan, J., Lunch, C.K., Neilson, R.P., Sheridan, S.C., Verville, J.H., 2004. Emissions pathways, climate change, and impacts on California. Proceedings of the National Academy of Sciences. 101,pp. 12422–12427. https://doi.org/10.1073/pnas.0404500101.
Heiman, D., Knecht, M.L., 2011. A Roadmap to Watershed Management: Sacramento Valley Subregion.
Hong, S.-Y., Pan, H.-L., 1996. Nonlocal boundary layer vertical diffusion in a medium-range forecast model. Mon. Weather Rev. 124,2322–2339. https://doi.org/10.1175/1520-0493(1996)124<2322:NBLVDI>2.0.CO;2.
Horne, F.E., Kavvas, M.L., 1997. Physics of the spatially averaged snowmelt process. J. Hydrol. 191 (1), 179–207.
Intergovernmental Panel on Climate Change, 2013. In: Stocker, T.F., Qin, D., Plattner, G.K., MMB, Tignor, Allen, S.K., Boschung, J., Nauels, A., Xia, Y., Bex, V., Midgley, P.M. (Eds.), Climate Change 2013: The Physical Science Basis, p. 1535.
Ishida, K., Kavvas, M.L., Jang, S., 2015a. Comparison of Performance on Watershed-Scale Precipitation between WRF and MM5. American Society of Civil Engineers, pp. 989–993.
Ishida, K., Kavvas, M.L., Jang, S., Chen, Z.Q., Ohara, N., Anderson, M.L., 2015b. Physically based estimation of maximum precipitation over three watersheds in Northern California: atmospheric boundary condition shifting. J. Hydrol. Eng. 20, 04014052. https://doi.org/10.1061/(ASCE)HE.1943-5584.0001026.
Ishida, K., Kavvas, M.L., Jang, S., Chen, Z.Q., Ohara, N., Anderson, M.L., 2015c. Physically based estimation of maximum precipitation over three watersheds in Northern California: relative humidity maximization method. J. Hydrol. Eng., 04015014 https://doi.org/10.1061/(ASCE)HE.1943-5584.0001175.
Jones, R.G., Murphy, J.M., Noguer, M., 1995. Simulation of climate change over europe using a nested regional-climate model. I: assessment of control climate, including sensitivity to location of lateral boundaries. Q. J. R. Meteorol. Soc. 121,1413–1449. https://doi.org/10.1002/qj.49712152610.
Kain, J.S., Fritsch, J.M., 1993. Convective parameterization for mesoscale models: The Kain-Fritsch scheme. In: Emanuel, K.A., Raymond, D.J. (Eds.), The Representation of Cumulus Convection in Numerical Models. American Meteorological Society, pp. 165–170.
Kapnick, S., Hall, A., 2010. Observed climate-snowpack relationships in California and their implications for the future. J. Clim. 23, 3446–3456.
Khadka, D., Babel, M.S., Shrestha, S., Tripathi, N.K., 2014. Climate change impact on glacier and snow melt and runoff in Tamakoshi basin in the Hindu Kush Himalayan (HKH) region. J. Hydrol. 511,49–60. https://doi.org/10.1016/j.jhydrol.2014.01.005.
Kumar, S., Merwade, V., Kinter, J.L., Niyogi, D., Kumar, S., Merwade, V., III, J.L.K., Niyogi, D., 2013. Evaluation of temperature and precipitation trends and long-term persistence in CMIP5 twentieth-century climate simulations. J. Clim. 26,4168–4185. https://doi.org/10.1175/JCLI-D-12-00259.1.
Lin, Y., Ba, Colle, Yuter, S.E., 2013. Impact of moisture flux and freezing level on simulated orographic precipitation errors over the Pacific Northwest. J. Hydrometeorol. 14,140–152. https://doi.org/10.1175/JHM-D-12-019.1.
Martinec, J., 1960. The Degree-Day Factor for Snowmelt Runoff Forecasting. IUGG General Assembly of Helsinki. IAHS Commission of Surface Waters, pp. 468–477.
Martinec, J., Rango, A., 1981. Areal distribution of snow water equivalent evaluated by snow cover monitoring. Water Resour. Res. 17, 1480–1488.
Mass, C.F., Ovens, D., Westrick, K., Colle, B.A., 2002. Does increasing horizontal resolution produce more skillful forecasts? Bull. Am. Meteorol. Soc. 83,407–430. https://doi.org/10.1175/1520-0477(2002)083<0407:DIHRPM>2.3.CO;2.
Maurer, E.P., 2007. Uncertainty in hydrologic impacts of climate change in the Sierra Nevada, California, under two emissions scenarios. Clim. Chang. 82,309–325. https://doi.org/10.1007/s10584-006-9180-9.
McAfee, S.A., Walsh, J., Rupp, T.S., 2014. Statistically downscaled projections of snow/rain partitioning for Alaska. Hydrol. Process. 28,3930–3946. https://doi.org/10.1002/hyp.9934.
Minder, J.R., Kingsmill, D.E., 2013. Mesoscale variations of the atmospheric snow line over the Northern Sierra Nevada: multiyear statistics, case study, and mechanisms. J. Atmos. Sci. 70,916–938. https://doi.org/10.1175/JAS-D-12-0194.1.
Minder, J.R., Durran, D.R., Roe, G.H., 2011. Mesoscale controls on the mountainside snow line. J. Atmos. Sci. 68,2107–2127. https://doi.org/10.1175/JAS-D-10-05006.1.
Moss, R.H., Edmonds, J.A., Hibbard, K.A., Manning, M.R., Rose, S.K., van Vuuren, D.P., Carter, T.R., Emori, S., Kainuma, M., Kram, T., Meehl, G.A., Mitchell, J.F.B., Nakicenovic, N., Riahi, K., Smith, S.J., Stouffer, R.J., Thomson, A.M., Weyant, J.P., Wilbanks, T.J., 2010. The next generation of scenarios for climate change research and assessment. Nature 463,747–756. https://doi.org/10.1038/nature08823.
Nakicenovic, N., Swart, R., 2000. Special report on emissions scenarios. Special Report on Emissions Scenarios, Edited by Nebojsa Nakicenovic and Robert Swart. 1. Cambridge University Press, Cambridge, UK, p. 612 July 2000. ISBN 0521804930.
National Marine Fisheries Service (NMFS), 2000. National Marine Fisheries Service. Public Draft Central Valley Recovery Plan. Appendix A: Central Valley Watershed Profiles. NOAA Fisheries Service.
NCAR, 2005. PSU/NCAR Mesoscale Modeling System Tutorial Class Notes and User's Guide: MM5 Modeling System Version 3. pp. 8–13.
Ohara, N., Kavvas, M.L., 2006. Field observations and numerical model experiments for the snowmelt process at a field site. Adv. Water Resour. 29,194–211. https://doi.org/10.1016/j.advwatres.2005.03.016.
Ohara, N., Kavvas, M.L., Kure, S., Chen, Z.Q., Jang, S., Tan, E., 2011. Physically based estimation of maximum precipitation over American River Watershed, California. J. Hydrol. Eng. 16,351–361. https://doi.org/10.1061/(asce)he.1943-5584.0000324.
Pons, M.R., San-Martín, D., Herrera, S., Gutiérrez, J.M., 2009. Snow trends in Northern Spain: analysis and simulation with statistical downscaling methods. Int. J. Climatol. https://doi.org/10.1002/joc.2016 (n/a-n/a).
Rango, A., Martinec, J., 1995. Revisiting the degree-day method for Computations1. J. Am. Water Resour. Assoc. 31, 657–669.
Reisner, J., Rasmussen, R.M., Bruintjes, R.T., 1998. Explicit forecasting of supercooled liquid water in winter storms using the MM5 mesoscale model. Q. J. R. Meteorol. Soc. 124,1071–1107. https://doi.org/10.1002/qj.49712454804.
Roeckner, E., Bäuml, G., Bonaventura, L., Brokopf, R., Esch, M., Giorgetta, M., Hagemann, S., Kirchner, I., Kornblueh, L., Rhodin, A., Schlese, U., Schulzweida, U., Tompkins, A., 2003. The Atmospheric General Circulation Model ECHAM5: Part 1: Model Description. MPI Report. 349 pp. 1–140.
Serreze, M.C., Clark, M.P., Armstrong, R.L., Da, McGinnis, Pulwarty, R.S., 1999. Characteristics of the western United States snowpack from snowpack telemetry (SNOTEL) data. Water Resour. Res. 35,2145–2160. https://doi.org/10.1029/1999WR900090.
Soong, S.-T., Kim, J., 1996. Simulation of a heavy wintertime precipitation event in California. Clim. Chang. 32,55–77. https://doi.org/10.1007/BF00141278.
Stewart, I.T., Cayan, D.R., Dettinger, M.D., 2004. Changes in snowmelt runoff timing in western North America under abusiness as usual'climate change scenario. Clim. Chang. 62, 217–232.
Trinh, T., Kavvas, M.L., Ishida, K., Carr, K., Ohara, N., 2017. Projected 21st century climate change on snow conditions over Shasta Dam watershed by means of dynamical downscaling. Hydrol. Process. 31,2887–2901. https://doi.org/10.1002/hyp.11231.
U.S. Fish and Wildlife Service (USFWS), 1995. Working Paper on Restoration Needs: Habitat Restoration Actions to Double Natural Production of Anadromous Fish in the Central Valley of California. Vol. 2.
Vicuna, S., Dracup, J., 2007. The evolution of climate change impact studies on hydrology and water resources in California. Clim. Chang. 82, 327–350.